RESEARCH ARTICLE | JUNE 22 2020

Reversible transition between bipolar resistive switching and threshold switching in 2D layered III–VI semiconductor GaSe

Huiying Du; Meilin Tu; Songwen Luo; Yuhuan Liu; Xinyue Qiu; Haipeng Lu; Shangdong Li ; Shuoguo Yuan; Wen Huang; Wenjing Jie ; Jianhua Hao

Appl. Phys. Lett. 116, 253102 (2020)
https://doi.org/10.1063/5.0010498

Applied Physics Letters ARTICLE scitation.org/journal/apl

Reversible transition between bipolar resistive switching and threshold switching in 2D layered III–VI semiconductor GaSe

Cite as: Appl. Phys. Lett. **116**, 253102 (2020); doi: 10.1063/5.0010498
Submitted: 11 April 2020 · Accepted: 9 June 2020 ·
Published Online: 22 June 2020

Huiying Du,[1] Meilin Tu,[1] Songwen Luo,[1] Yuhuan Liu,[1] Xinyue Qiu,[1] Haipeng Lu,[2] Shangdong Li,[3] Shuoguo Yuan,[4] Wen Huang,[3] Wenjing Jie,[1,a)] and Jianhua Hao[4,a)]

AFFILIATIONS

[1]College of Chemistry and Materials Science, Sichuan Normal University, Chengdu 610066, China
[2]National Engineering Research Center of Electromagnetic Radiation Control Materials, University of Electronic Science and Technology of China, Chengdu 610054, China
[3]State Key Laboratory of Electronic Thin Films and Integrated Devices, School of Electronic Science and Engineering, University of Electronic Science and Technology of China, Chengdu 610054, China
[4]Department of Applied Physics, The Hong Kong Polytechnic University, Hung Hom, Kowloon, Hong Kong, China

[a)]**Authors to whom correspondence should be addressed:** wenjing.jie@sicnu.edu.cn and jh.hao@polyu.edu.hk

ABSTRACT

Recently, two-dimensional (2D) layered materials have emerged as promising candidates for resistive switching (RS) devices. However, challenges in controllable conversion of RS types in such 2D materials still remain. Here, we report the experimental realization of reversible transition between non-volatile bipolar resistive switching (BRS) and volatile threshold switching (TS) in 2D layered III–VI semiconductor gallium selenide (GaSe) nanosheets through appropriately setting the compliance current (I_{cc}). Under a relatively high I_{cc} value of 1 mA, the device shows non-volatile BRS performance with a high ON/OFF ratio of nearly 10^4, a long retention time of 12 000 s, and a high endurance of 1200 switching cycles. Furthermore, under a relatively low I_{cc} (lower than 10 μA), the volatile TS behaviors can be observed. For the former, the large I_{cc} can generate stable conductive filaments (CFs) of Ga vacancy. Thus, the breakage of the stable CFs needs a high reverse voltage to re-align the Ga vacancy. For the latter, the low I_{cc} generated unstable CFs can be broken by the current induced Joule heat. This study establishes the feasibility of integrating different RS types in 2D layered semiconductor nanosheets and understanding the underlying physical mechanism of different RS types in the 2D platform.

Resistive switching (RS) devices have drawn much attention owing to their high performances including non-volatility, low power consumption, fast switching speed, and large storage capability.[1] Generally, they are two-terminal devices with a vertical sandwich structure by integrating an switching layer of an insulator or a semiconductor sandwiched between two metal electrodes. According to switching characteristics, RS can be divided into two types, namely, non-volatile RS and volatile threshold switching (TS). For non-volatile RS, the high resistance state (HRS) and low resistance state (LRS) can be maintained even after removing the external voltage until a reverse large voltage is applied. For TS, only the HRS is stable with the absence of external voltage.[2,3] The former as non-volatile memory can be used for computing and the recently developed multifunctional synaptic neurons, while the latter can be employed for crosstalk current suppression in cross arrays.[4,5] In recent years, some research groups have reported that the two types of RS behaviors could coexist or transform to each other in a single device with appropriate external stimulations. The transition can generally be achieved by setting different compliance currents (I_{cc}), which can trigger various types of RS states in some oxide thin films, such as SiO_2,[3] NiO_2,[4] HfO_x,[6] NbO_x,[7] and MnO.[8] Moreover, our research group found a transition from non-volatile bipolar resistive switching (BRS) to volatile TS behaviors by changing the electrode from Au to Ag in a single MoO_3 nanobelt.[9]

Diverse materials have been used to serve as the RS layer to date. Among them, two-dimensional (2D) layered materials have recently drawn much attention in RS devices ever since monolayer MoS_2 exhibited gate-tunable RS properties reported by Sangwan in 2015.[10] After that, a series of 2D materials have been employed in RS devices,

ranging from graphene to graphene oxide,[11–13] transition metal dichalcogenides (TMDs), and hexagonal boron nitride (*h*-BN).[14–17] Specifically, the intriguing transition between non-volatile RS and volatile TS was also reported in 2D layered *h*-BN insulators.[18,19] However, major challenges in reversible conversion between RS and TS in other 2D materials particularly 2D semiconductors that are more useful in electronics still remain.[20] Among 2D layered materials, GaSe is a typical III–VI layered semiconductor with *p*-type properties.[21–23] Recently, our research group has studied the gate-tunable RS properties of 2D GaSe nanosheets with Ag electrodes.[24] The GaSe nanosheets exhibited excellent RS performances, suggesting promising applications in multi-terminal electronic devices with complex functionalities and low power consumption. In this work, we report a controllable conversion between BRS and TS in mechanically exfoliated 2D GaSe nanosheets. The inert metal of Au is employed to fabricate lateral RS devices, which fully excludes the possibility of forming metal filaments. This work would help one to investigate complex RS types based on 2D layered semiconductors and to understand the underlying physical mechanism of different RS types in 2D nanosheets.

2D layered GaSe nanosheets were prepared by the mechanical exfoliation method and then transferred onto the Si substrates covered by a 300 nm SiO_2 layer. The detailed exfoliation and transferring methods can be referred to our earlier work.[24] For device fabrication, a shadow mask with a stripe pattern was carefully mounted on the GaSe nanosheets under an optical microscope. Au electrodes with a thickness of ∼100 nm were deposited by the sputtering method to form two terminal Au/GaSe/Au devices for RS measurements, as schematically shown in Fig. 1(a). The distance between the two adjacent strip Au electrodes is ∼30 μm. The surface morphology and thickness of GaSe nanosheets were confirmed by atomic force microscopy (AFM, DI Nanocope 8). A Raman spectroscope with a laser wavelength of 633 nm and a spot size of ∼1 μm (HORIBA JOBIN YVON, HR800) was used to characterize the prepared GaSe nanosheets. The electrical characteristics of RS devices were tested using a double channel Keithley 2636B SourceMeter with a four-probe station. All measurements were performed at room temperature in air.

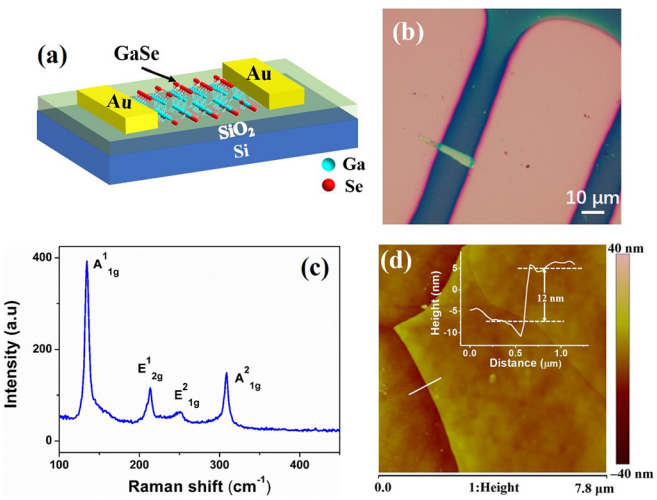

FIG. 1. (a) Schematic of the fabricated Au/GaSe/Au lateral RS device. (b) Optical image of the RS device. (c) Raman spectrum of the 2D GaSe nanosheet. (d) AFM image of the 2D GaSe nanosheet.

Figure 1(b) shows the optical micrograph of the two-terminal device for a good understanding of the Au/GaSe/Au structure. The Raman spectrum, as shown in Fig. 1(c), demonstrates the feature peaks of GaSe, including three strong peaks of A^1_{1g} mode (134.49 cm^{-1}), E^1_{2g} mode (213.53 cm^{-1}), and A^2_{1g} mode (308.87 cm^{-1}), as well as one weak peak of E^2_{1g} mode (250 cm^{-1}). All the Raman feature peaks are consistent with those of previously studied GaSe nanosheets prepared by the exfoliation method.[21] Besides, the AFM image shows that the morphology of the GaSe flake is smooth, as shown in Fig. 1(d). The Raman and AFM characterization studies indicate that the GaSe nanosheets have been well exfoliated and transferred onto the target substrate. The inset in Fig. 1(d) shows the AFM height profile, suggesting that the flake thickness is ∼12 nm, corresponding to the layer number of ∼15.[25] In our experiments, the GaSe nanosheets with a thickness of ∼12 nm were selected to fabricate RS devices in order to obtain comparable RS properties in different devices.

The RS properties of GaSe nanosheets were measured based on the lateral Au/GaSe/Au structure at room temperature. The inert metal of Au is used, which fully excludes the possibility of forming the metal filaments. An I_{cc} value of 1 mA was applied during the measurement to avoid damage of the device. Initially, the device does not show the typical current–voltage (*I*–*V*) characteristics of RS. The initial *I*–*V* loop is shown in the inset of Fig. 2(a). In our experiments, several scanning loops with an operating voltage of 1 V were needed prior to the appearance of a typical non-volatile BRS *I*–*V* curve, which corresponds to the forming process. After that, the device shows typical BRS behaviors, as shown in Figs. 2(a) and 2(b). The device is initially in the HRS. When a positive bias sweep is applied, the current suddenly increases from 10^{-8} to 10^{-3} A at a voltage around 0.23 V, inducing the SET process of switching from the HRS to LRS. The LRS can be maintained

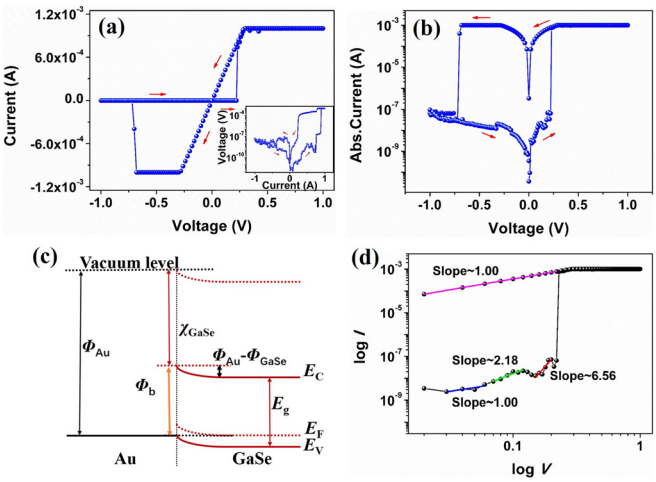

FIG. 2. The RS behaviors of GaSe nanosheets with the I_{cc} value of 1 mA. (a) Typical *I*–*V* curve of the Au/GaSe/Au devices in double linear coordinates. The inset shows the initial *I*–*V* curve of the device. (b) The typical *I*–*V* curve with current in the logarithmic coordinate. The arrows show the sweep directions of the voltage. (c) The energy band diagram of GaSe in contact with the Au electrode, in which E_V, E_C, and E_F represent the valence band, conduction band, and Fermi energy level of GaSe, respectively. (d) The positive *I*–*V* curve in double logarithmic coordinates.

during the subsequent positive scanning and the initial reverse negative scanning. When the negative voltage increases up to – 0.72 V in the reverse scanning process, the device can be switched back to the HRS, i.e., RESET process. The sharp current transition in both SET and RESET processes gives rise to a high resistance ON/OFF ratio up to 3.45×10^4 at a low SET voltage (V_{SET}) of ∼0.23 V. Due to the large channel length (∼30 μm), an ultralow SET electric field (E_{SET}) (∼77 V cm^{-1}) is achieved. The ultralow E_{SET} in 2D layered GaSe can also be found in our previously reported Ag/GaSe/Ag based RS device.[24] Besides, to further show the repeatable BRS characteristics, the *I*–*V* curves for 1, 10, 100, and 1000 cycles are demonstrated in Fig. S1(a). The GaSe based memristor shows reproducible BRS behaviors with V_{SET} changing from 0.2 to 0.8 V and the RESET voltage (V_{RESET}) changing from – 0.3 to – 0.8 V.

Furthermore, it is interesting to find that V_{SET} (∼0.23 V and E_{SET} ∼ 77 V cm^{-1}) in this work is much lower than that of our previously studied GaSe with an Ag electrode (1 V and 330 V cm^{-1}). To understand the mechanism behind the observed difference, we carefully analyze the electronic band structures of GaSe and Au. For *p*-type GaSe nanosheets, the electron affinity (χ_{GaSe}) is ∼3.1 eV with a bandgap of ∼2 eV and the ionization energy (E_{ion}) is ∼5.1 eV.[26] Thus, the Fermi energy (E_F) of *p*-type GaSe should be slightly smaller than 5.1 eV. The work function (Φ) of Au is 5.1 eV. Thus, nearly Ohmic contact can be formed between GaSe and Au, as shown in Fig. 2(c). However, for Ag with a work function of 4.26 eV, a Schottky barrier can be constructed between GaSe and Ag. The detailed information of the Ag/GaSe Schottky barrier was discussed in our previous work.[24] In the Ag/GaSe/Ag structure, the overall resistance consists of three parts, GaSe and two junctions of Ag/GaSe. Thus, there should be a large portion of external voltage dropped on the Schottky barrier (Ag/GaSe) when the bias voltage is applied on the device. However, for Au electrodes, the majority of the external voltage is applied on the GaSe layer rather than the Au/GaSe junction. Therefore, the low V_{SET} (E_{SET}) of the Au/GaSe/Au device is due to the low migration energy of the Ga vacancy in *p*-type GaSe and the nearly Ohmic contact between Au electrodes and the GaSe nanosheets.

To further understand the *I*–*V* curve of the device, the positive voltage part is re-plotted in double logarithmic coordinates, as shown in Fig. 2(d). The linear fitting curve can be divided into four regions under forward scanning. At very small voltages ($V < 0.06$ V), the fitting slope of the HRS is 1.00, indicating the nature of Ohmic contact. This is also consistent with the aforementioned analysis of Au/GaSe band structures. As the voltage increases, the slope rapidly increases to 2.18 ($0.06\ \text{V} < V < 0.12$ V) and finally to 6.56 ($0.12\ \text{V} < V < 0.23$V). Furthermore, the *I*–*V* curves of 10 and 100 cycles are carefully analyzed in double logarithmic coordinates (see Fig. S2). The linear fitting data with the slopes changing from initial ∼1, then to ∼2, and finally to one in excess of 2 at the HRS show similar trends as seen in Fig. 2(d), indicating that the slopes are reproducible for multiple switching cycles. This is the typical transport characteristic of space charge limited current (SCLC) injection.[27,28] Then, the device is shifted to the LRS with the slope of 1.00, indicating the Ohmic contact behavior, suggesting the formation of the conductive filaments (CFs) in the LRS. To fully understand the BRS mechanism, the cartoon of the switching mechanism is plotted, as shown in Fig. S3. 2D layered GaSe is of *p*-type with the carrier of the Ga vacancies.[29,30] The *p*-type behaviors can be confirmed by the transport properties of the 2D layered GaSe nanosheets (see Fig. S4). Thus, the Ga vacancy is proposed to be responsible for the observed BRS behaviors in the GaSe nanosheets. When a positive voltage larger than V_{SET} is applied, the Ga vacancies can be accumulated at the electrode vicinity and form the CFs, giving rise to the observed LRS. When a negative voltage in excess of V_{RESET} is applied, the accumulation of Ga vacancies at the vicinity of the electrode is decreased, inducing the breakage of the CFs.

Then, the retention and endurance characteristics of the Au/GaSe/Au device were measured at room temperature. Figure 3(a) shows the retention performance of the device by applying 1 V and –1 V pulse voltages with a duration of 0.1 s as V_{SET} and V_{RESET}, respectively. The read voltages of both the HRS and LRS are 0.2 V. The HRS and LRS of the device can be maintained up to 12 000 s without any decay or overlap between the HRS and LRS. During the overall retention period, the ON/OFF ratio can be well maintained with a value larger than 10^3. Moreover, the power-law extrapolation implies that the HRS/LRS switching ratio of the device can still be expected to be larger than 10^3even after 10 years, suggesting its excellent stability and retention performance (see Fig. S5). Figure 3(b) represents the endurance characteristics of the device. The device is tested under repetitive pulses with a duration of 0.1 s and a magnitude of 1 V for V_{SET} and –1 V for V_{RESET}. The HRS and LRS can be maintained with the RS ratio larger than 10^3 for over 1200 switching cycles, implying good reproducibility and reliability of the device for potential memory applications.

Furthermore, when I_{cc} decreases to100 μA, the device still exhibits typical non-volatile BRS characteristics, as shown in Fig. S6(a). The device shows the BRS *I*–*V* curve similar to that under the I_{cc} value of 1 mA. Figure S6(b) shows the linear fitting image of the positive *I*–*V* curve in double-logarithmic coordinates. The *I*–*V* curve in the HRS can be divided into three periods with the slope of 1.00, 1.77, and 2.73, respectively. For the LRS, the slope of the linear fitting is 1.00. These fitting data are consistent with the *I*–*V* curve under the I_{cc} value of 1 mA. When I_{cc} is further decreased to 10 μA [Fig. 4(a)], the device shows dramatic changes, from the non-volatile BRS to the volatile TS behaviors. Through a scanning of positive voltage, the initial HRS can be switched to the LRS. However, the LRS cannot be maintained. The LRS is switched into the HRS when the positive voltage is removed. For scanning of negative voltage, the device exhibits a nearly symmetric switching loop to that of the positive voltage scanning, indicating that the device has typical bi-directional volatile TS characteristics. Furthermore, we recorded 100 cycles of the TS behaviors with the I_{cc} value of 10 μA in our experiments, as shown in Fig. S7 of the *I*–*V* curves for 1, 10, and 100 cycles. The device shows good repeatability of

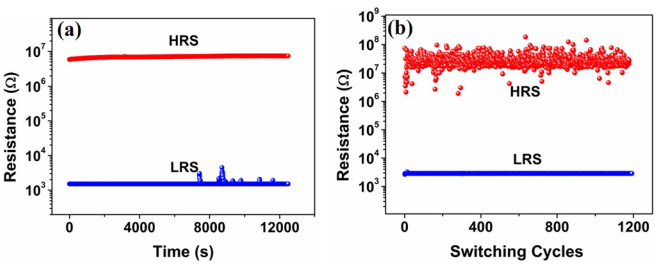

FIG. 3. (a) Retention characteristics of the Au/GaSe/Au device with 1 mA compliance current. (b) Cycle endurance characterization of the device.

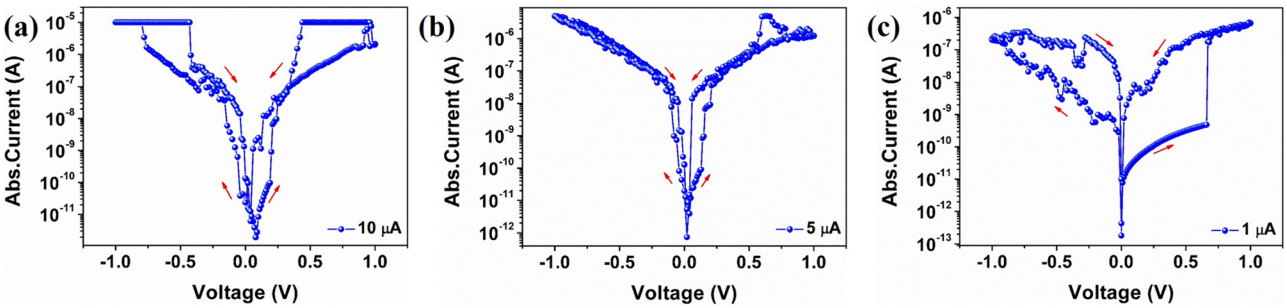

FIG. 4. The RS behaviors of GaSe nanosheets with the relatively low I_{cc} of (a) 10 μA, (b) 5 μA, and (c) 1 μA.

the TS behaviors. Then, when I_{cc} is further decreased to 5 μA [Fig. 4(b)], the device exhibits a similar I–V curve to that with the I_{cc} value of 10 μA. When the I_{cc} value is decreased to 1 μA, the volatile TS behaviors can be maintained with the ON/OFF ratio of $\sim 10^2$ [Fig. 4(c)]. In our experiments, the volatile TS characteristics can be achieved at a relatively low I_{cc} ($\leq$10 μA), while the non-volatile BRS behaviors of the device can be triggered by a relatively high I_{cc} ($\geq$100 μA). Some previous studies reported that weak and discrete filaments can be generated in TS mode at the LRS.[3,31] When the device is at a relatively low I_{cc}, the formed CFs in the GaSe layer are unstable. Thus, the CFs can be spontaneously dissolved by the electric current induced Joule heat in the TS mode.[32–34] Accordingly, the device switches back to the HRS when the applied voltage is lower than the threshold voltage. On the other hand, the relatively high I_{cc} is beneficial for the generation of large and stable CFs. The electric current induced Joule heat is not sufficient to break the formed CFs. Thus, a reverse voltage is needed to re-align Ga vacancy and induce the breakdown of CFs in BRS mode. More importantly, when I_{cc} is gradually increased, a reverse transition from volatile TS to non-volatile RS can be observed (see Fig. S8). When I_{cc} is increased from 1 to 10 μA, the device shows volatile TS behaviors, consistent with those observed when I_{cc} is decreased from 10 to 1 μA. When I_{cc} is further increased to 100 μA, non-volatile RS behaviors arise. Therefore, the transition between non-volatile BRS and volatile TS is reversible and repeatable in 2D layered GaSe nanosheets by setting different I_{cc} values.

In summary, the controllable transition between volatile TS and non-volatile BRS can be realized in lateral two-terminal Au/GaSe/Au RS devices by appropriately setting I_{cc}. To be more specific, under the relatively high I_{cc}, the stable Ga vacancy CFs can be generated, and the device exhibits non-volatile bipolar BRS behaviors with high ON/OFF ratios up to 10^4 and a low V_{SET} of $\sim$0.23 V. On the other hand, under the relatively low I_{cc} ($\leq$10 μA), the weak and unstable CFs are formed in the GaSe nanosheets, giving rise to the volatile bidirectional TS behaviors. Furthermore, the RESET process in the BRS mode is different from that in the TS mode. For the former, the breakage of the CFs is caused by the migration of Ga vacancy to the reverse direction under the negative electric field, while the latter is caused by the spontaneous dissolution of the unstable CFs under Joule heat. The reversible conversion between the BRS and TS behaviors in 2D GaSe nanosheets provides one opportunity to integrate multifunctional performance in such a 2D platform.

See the supplementary material for additional characterization and electrical measurements of our devices.

This work was supported by the grants from the National Natural Science Foundation of China (Nos. 61804023, 61971108, and 61974097), the Open Foundation of State Key Laboratory of Electronic Thin Films and Integrated Devices (No. KFJJ201805), the Open Foundation of National Engineering Research Center of Electromagnetic Radiation Control Materials (No. ZYGX2019K003-1), Sichuan Youth Science and Technology Foundation (No. 2019JDJQ0052), the Key R&D Program of Sichuan Province (No. 2018GZ0527), and Hong Kong RGC GRF (No. PolyU 153023/18P).

DATA AVAILABILITY

The data that support the findings of this study are available from the corresponding author upon reasonable request.

REFERENCES

[1]C. Ahn, Z. Jiang, C.-S. Lee, H.-Y. Chen, J. Liang, L. S. Liyanage, and H. S. P. Wong, IEEE Trans. Electron Devices **62**, 2197 (2015).
[2]C. Zhang, J. Shang, W. Xue, H. Tan, L. Pan, X. Yang, S. Guo, J. Hao, G. Liu, and R. W. Li, Chem. Commun. **52**, 4828 (2016).
[3]H. Sun, Q. Liu, C. Li, S. Long, H. Lv, C. Bi, Z. Huo, L. Li, and M. Liu, Adv. Funct. Mater. **24**, 5679 (2014).
[4]Y. J. Baek, Q. Hu, J. W. Yoo, Y. J. Choi, C. J. Kang, H. H. Lee, S. H. Min, H. M. Kim, K. B. Kim, and T. S. Yoon, Nanoscale **5**, 772 (2013).
[5]S. H. Chang, S. B. Lee, D. Y. Jeon, S. J. Park, G. T. Kim, S. M. Yang, S. C. Chae, H. K. Yoo, B. S. Kang, M. J. Lee, and T. W. Noh, Adv. Mater. **23**, 4063 (2011).
[6]R. Midya, Z. Wang, J. Zhang, S. E. Savel'ev, C. Li, M. Rao, M. H. Jang, S. Joshi, H. Jiang, P. Lin, K. Norris, N. Ge, Q. Wu, M. Barnell, Z. Li, H. L. Xin, R. S. Williams, Q. Xia, and J. J. Yang, Adv. Mater. **29**, 1604457 (2017).
[7]S. K. Nandi, X. Liu, D. K. Venkatachalam, and R. G. Elliman, J. Phys. D: Appl. Phys. **48**, 195105 (2015).
[8]H. Abbas, A. Ali, J. Jung, Q. Hu, M. R. Park, H. H. Lee, T.-S. Yoon, and C. J. Kang, Appl. Phys. Lett. **114**, 093503 (2019).
[9]H. Du, J. Chen, M. Tu, S. Luo, S. Li, S. Yuan, T. Gong, W. Huang, W. Jie, and J. Hao, J. Mater. Chem. C **7**, 12160 (2019).
[10]V. K. Sangwan, D. Jariwala, I. S. Kim, K. S. Chen, T. J. Marks, L. J. Lauhon, and M. C. Hersam, Nat. Nanotechnol. **10**, 403 (2015).
[11]C. He, Z. Shi, L. Zhang, W. Yang, R. Yang, D. Shi, and G. Zhang, ACS Nano **6**, 4214 (2012).
[12]S. K. Kim, J. Y. Kim, S.-Y. Choi, J. Y. Lee, and H. Y. Jeong, Adv. Funct. Mater. **25**, 6710 (2015).
[13]W. Lv, H. Wang, L. Jia, X. Tang, C. Lin, L. Yuwen, L. Wang, W. Huang, and R. Chen, ACS Appl. Mater. Interface **10**, 6552 (2018).
[14]P. Cheng, K. Sun, and Y. H. Hu, Nano Lett. **16**, 572 (2016).

[15]D. Li, B. Wu, X. Zhu, J. Wang, B. Ryu, W. D. Lu, W. Lu, and X. Liang, ACS Nano **12**, 9240 (2018).
[16]K. Qian, R. Y. Tay, V. C. Nguyen, J. Wang, G. Cai, T. Chen, E. H. T. Teo, and P. S. Lee, Adv. Funct. Mater. **26**, 2176 (2016).
[17]B. Wang, H. Luo, X. Wang, E. Wang, Y. Sun, Y. C. Tsai, H. Zhu, P. Liu, K. Jiang, and K. Liu, ACS Nano **14**, 175 (2020).
[18]C. Pan, Y. Ji, N. Xiao, F. Hui, K. Tang, Y. Guo, X. Xie, F. M. Puglisi, L. Larcher, E. Miranda, L. Jiang, Y. Shi, I. Valov, P. C. McIntyre, R. Waser, and M. Lanza, Adv. Funct. Mater. **27**, 1604811 (2017).
[19]A. Ranjan, N. Raghavan, S. J. O'Shea, S. Mei, M. Bosman, K. Shubhakar, and K. L. Pey, Sci. Rep. **8**, 2854 (2018).
[20]Y. Qiao, T. Hirtz, F. Wu, G. Deng, X. Li, Y. Zhi, H. Tian, Y. Yang, and T.-L. Ren, ACS Appl. Electron. Mater. **2**, 346 (2020).
[21]W. Jie, X. Chen, D. Li, L. Xie, Y. Y. Hui, S. P. Lau, X. Cui, and J. Hao, Angew. Chem. Int. Ed. **54**, 1185 (2015).
[22]W. Jie, Z. Yang, G. Bai, and J. Hao, Adv. Opt. Mater. **6**, 1701296 (2018).
[23]Z. Yang, Z. Wu, Y. Lyu, and J. Hao, InfoMat **1**, 98 (2019).
[24]Y. Yang, H. Du, Q. Xue, X. Wei, Z. Yang, C. Xu, D. Lin, W. Jie, and J. Hao, Nano Energy **57**, 566 (2019).
[25]Y. Zhou, Y. Nie, Y. Liu, K. Yan, J. Hong, C. Jin, Y. Zhou, J. Yin, Z. Liu, and H. Peng, ACS Nano **8**, 1485 (2014).
[26]R. Schlaf, O. Lang, C. Pettenkofer, and W. Jaegermann, J. Appl. Phys. **85**, 2732 (1999).
[27]D. Liu, H. Cheng, G. Wang, X. Zhu, and N. Wang, J. Appl. Phys. **114**, 154906 (2013).
[28]Y.-S. Fan, P.-T. Liu, L.-F. Teng, and C.-H. Hsu, Appl. Phys. Lett. **101**, 052901 (2012).
[29]P. Hu, Z. Wen, L. Wang, P. Tan, and K. Xiao, ACS Nano **6**, 5988 (2012).
[30]D. J. Late, B. Liu, J. Luo, A. Yan, H. S. S. R. Matte, M. Grayson, C. N. R. Rao, and V. P. Dravid, Adv. Mater. **24**, 3549 (2012).
[31]H. Wang, Y. Du, Y. Li, B. Zhu, W. R. Leow, Y. Li, J. Pan, T. Wu, and X. Chen, Adv. Funct. Mater. **25**, 3825 (2015).
[32]C. P. Hsiung, H. W. Liao, J. Y. Gan, T. B. Wu, J. C. Hwang, F. Chen, and M. J. Tsai, ACS Nano **4**, 5414 (2010).
[33]S. H. Chang, S. C. Chae, S. B. Lee, C. Liu, T. W. Noh, J. S. Lee, B. Kahng, J. H. Jang, M. Y. Kim, D. W. Kim, and C. U. Jung, Appl. Phys. Lett. **92**, 183507 (2008).
[34]S. H. Chang, J. S. Lee, S. C. Chae, S. B. Lee, C. Liu, B. Kahng, D. Kim, and T. W. Noh, Phys. Rev. Lett. **102**, 026801 (2009).